PHYSICAL REVIEW B **90**, 041409(R) (2014)

Sliding speed-induced nanoscale friction mosaicity at the graphite surface

M. V. Rastei,* P. Guzmán, and J. L. Gallani
Institut de Physique et Chimie des Matériaux de Strasbourg, CNRS, Université de Strasbourg, F-67034 Strasbourg, France
(Received 7 March 2014; revised manuscript received 16 June 2014; published 21 July 2014)

The kinetic friction of the (0001) graphite surface has been mapped at different speeds and scales by means of an atomic force microscope. The maps show nanoscale domains of various sizes and friction strengths. Each domain presents a transition between two friction regimes and a specific logarithmic scaling of friction with speed. The gradient of this variation is determined by the angle between the macroscopic sliding direction and a stiff crystal axis of the surface lattice. The experimental results are analyzed by considering thermally activated sliding regimes within the puckering friction mechanism.

DOI: 10.1103/PhysRevB.90.041409 PACS number(s): 46.55.+d, 61.72.Hh, 62.20.Qp, 81.05.uf

When two bodies frictionally slide on each other, interfacial asperities experience lateral potential barriers. Such a barrier is surmounted by converting part of the kinetic energy of the sliding body into potential energy. On the other side of the barrier the potential energy partly transforms into heat which then dissipates towards the bulks [1]. These processes, central to sliding friction, inextricably depend on contact mechanics [2], but also on external parameters such as temperature and speed. The impact of these two competing factors on friction has primarily been modeled for atomic scale contacts [3–6]. Far less is known, however, about temperature and speed dependence of friction in larger contacts made by means of several atoms at a time [7–9].

Graphite and graphitic materials in general are known as excellent dry lubricants. Recent friction experiments, however, demonstrate that the friction characteristics of these materials are far from being fully understood [10–16]. On graphene samples for instance, a recent study revealed an unexpected nanoscale friction mechanism, based on a puckering effect in front of a sliding tip [17]. The mechanism was then used to explain intriguing friction anisotropies on graphite and graphene surfaces [10,18]. While these studies clearly indicate that the puckering effect alters friction at the surface of layered materials, the impact of the sliding speed has not yet been addressed. Here we report the speed-induced observation of a wide range of frictional domains at the graphite surface. We show that each domain presents a particular logarithmic dependence of friction with speed, indicating a thermally assisted sliding implying different potential barriers. The difference is proposed to arise from the way the tip interacts with the ridge of the puckered region, which in turn depends on a stiff crystal axis settled by structural defects.

The measurements were performed with an atomic force microscope (AFM) operating below 10^{-4} mbar and at room temperature. The (0001) surface of highly oriented pyrolytic graphite (HOPG) was cleaned by repeated exfoliations. The friction force microscopy (FFM) signal was recorded while scanning along the cantilever axis. We used silicon AFM probes with original tip radii of about 10 nm. The normal and lateral spring constants of the probes were of the order of 0.01 and 20 N/m, respectively. All data reported here were obtained with a constant normal load of 0.5 nN. Before gathering data, the tip was treated *in situ* by scanning at high speeds, and loads up to 3 nN. The tips processed in this way are most likely blunter but they provide more reproducible measurements.

Figure 1(a) shows a large scale FFM image acquired at the graphite surface with 2.4 μm/s. The image reveals domains of various shapes and sizes and a wide range of friction contrasts. The domains are generally—but not always—delimited by atomic steps formed during the exfoliation process: A domain can extend over several atomic terraces, whereas in other places multiple domains can occupy an atomically flat terrace. In Fig. 1(a) two polygons show such configurations as examples.

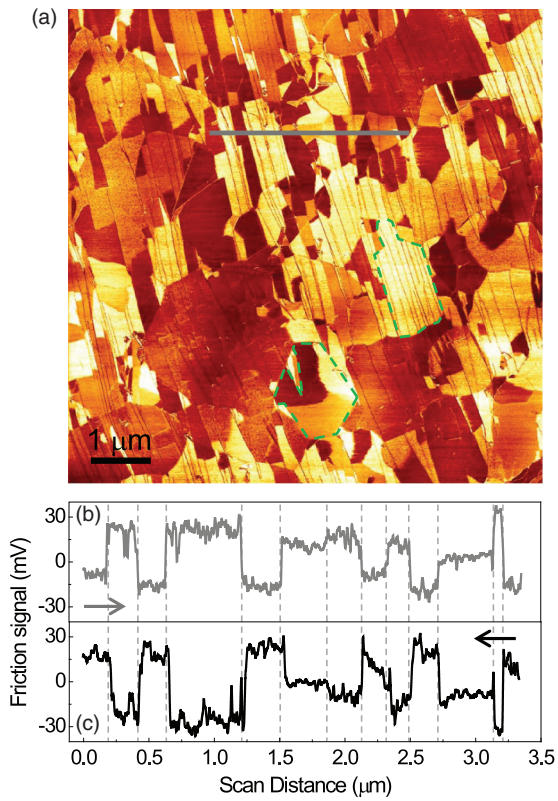

FIG. 1. (Color online) (a) FFM forward image (8×8 μm^2) of a graphite surface reveling frictional domains of different sizes and shapes. The polygons delimit areas relevant for discussion in the text. Forward (b) and backward (c) scan profiles along the line shown in (a). Vertical lines mark domain boundaries.

*rastei@ipcms.unistra.fr

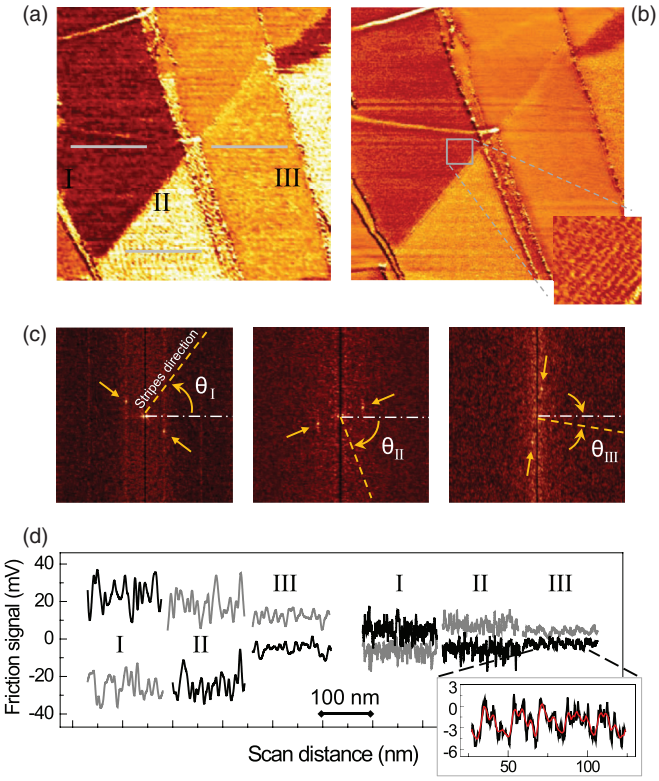

FIG. 2. (Color online) FFM forward images (500×500 nm^2) acquired at (a) 2.4 μm/s and (b) 0.2 μm/s. Both images span the same gray scale. The inset in (b) highlights the stripe pattern from domain I. (c) Fast Fourier transform (FFT) images obtained for the three domains from (b). The bright spots in the FFT images are generated by the periodicity of the stripes in each domain. The direction of the stripes with respect to the fast-scan direction is indicated by θ angles. (d) Forward (gray) and backward (black) scan profiles along the lines shown in (a) for 2.4 μm/s (left) and 0.2 μm/s (right). Inset: Close-view profile still exhibiting a stick-slip signal.

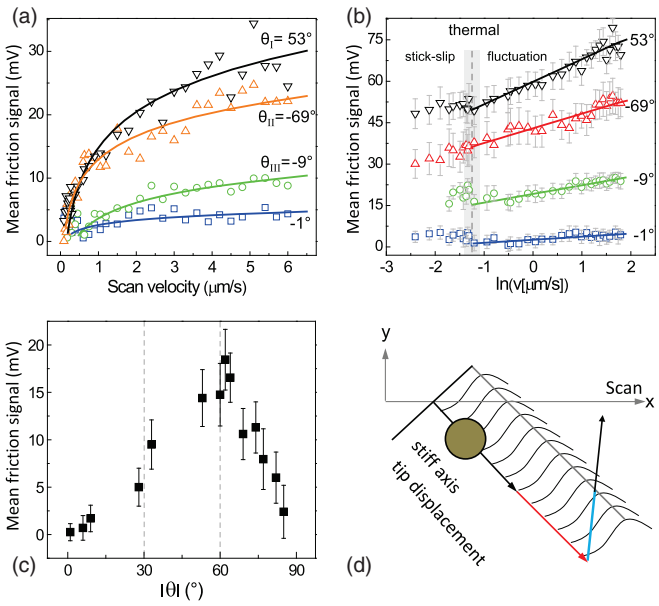

FIG. 3. (Color online) (a) Speed dependence of friction for domains identified in Fig. 2. The lowest curve corresponds to the zone located above domain III. Error bars are shown in (b). Solid lines are logarithmic fits through data points. (b) Same data as in (a) but as a function of $\ln v$. Data points are vertically shifted for clarity. The vertical mark indicates a transition from stick-slip to fluctuating signal. Solid lines are linear fits through data obtained at $v > v_t$. (c) Mean friction for various domains imaged at $v = 0.9$ μm/s. The θ angles were obtained from low-speed images. Error bars for θ are smaller than the size of the data points. (d) Drawing illustrating a surface puckering ridge as faced by the tip while displacing along the stiff axis. Red line indicates positions where a tip escape is expected. Blue segment depicts the distance to the top of the ridge.

Figures 1(b) and 1(c) depict profiles for forward and backward scans along the line from Fig. 1(a). The profiles reveal opposite signals of specific intensity for each domain. Although such domains resemble the ones observed for rippled graphene sheets [18,19], they originate here from the puckering friction induced by sliding tips [10,17]. The effect of puckering is checked by imaging small areas, and searching for stripes produced by the periodic relaxation of the puckered surface [10]. This is done for example in Fig. 2, where a closer look indeed reveals stripe patterns [inset Fig. 2(b)]. Interestingly, the stripes are well observed only for speeds below a certain threshold v_t (here $v_t = 0.28 \pm 0.05$ μm/s). For $v > v_t$, the stripes vanish rather rapidly. Instead, a larger and fluctuating friction signal sets in [Figs. 2(a) and 2(d)]. On domains imaged at $v < v_t$, fast Fourier transform (FFT) analyses can be used to obtain the direction (θ) of the stripes. This allows a labeling of domains. FFT images corresponding to the domains labeled in Fig. 2 are shown in Fig. 2(c). We get $\theta_I = 53°$, $\theta_{II} = -69°$, and $\theta_{III} = -9°$. Additionally, the angular difference $\Delta\theta_{II\text{-}I} = 122°$ indicate a 2° mismatch angle between the grains comprising domain I and II [20]. The separation between domain II and III is made by atomic steps. Hence, $\Delta\theta_{III\text{-}II} = 60°$ exactly reflects the symmetry of the surface.

Figures 3(a) and 3(b) show the speed dependence of friction computed as an average of forward and backward signals. For all domains the friction follows a logarithmic increase with speed. The semilog plot in Fig. 3(b) however displays a passage between two friction regimes. It corresponds to the threshold v_t, which falls at similar speeds for all domains. A slightly weaker friction is measured soon after the passage. Yet, a noticeable difference between domains stands in the gradient of the logarithmic variation. For domains with $0° < |\theta| < 60°$, the slope of the variation progressively rises up. The trend reverses for domains with $60° < |\theta| < 90°$. A way to further understand this change is to measure, at a fixed v, the friction on many domains and plot it as a function of θ [Fig. 3(c)]. As observed, friction increases until $|\theta|$ reaches 60°, and then it decreases when $|\theta|$ moves upwards to 90°. This, again, recalls the puckering friction, which relies on a defect-induced stiffness enhancement for one of the high-symmetry crystal axes [10]. In this respect, Fig. 3(d) illustrates a surface ridge formed along the stiffest crystal axis [21]. Therefrom, it can be deduced that the friction varies as the stiff axis—and hence the ridge of the puckered region—aligns with the scan direction. In fact, for each 60° a second axis of the same symmetry as the stiff axis enters the quadrant [22]. This may lift the

compliance of the surface inducing a weaker puckering and, as a consequence, a lower friction, as observed for angles above 60°. Note that for graphene the friction varies with a periodicity of 180°, due to linear intrinsic ripples induced by the substrate [18]. Here, on graphite, such ripples do not exist and so the angular dependence of friction is more subject to the hexagonal structure of the crystal lattice.

To gain insights into the origin of the observed speed behavior, we focus on the fluctuating friction profiles. In contrast with the friction signal reported in [10], where the relaxation of puckered region generates regular and sharp slip events, the fluctuating profiles observed here suggest a relaxation occurring to a lesser extent. This can primary be associated with the high sliding speeds but also with the likely larger tip radius. The tip continuously interacts thus with a tilted surface, experiencing a nonvanishing lateral force as observed in Fig. 2(d).

To further account for our experimental observations, we consider a speed-induced forward movement of the puckered region. In this picture, the threshold v_t, observed in Fig. 3(b), reflects the speed at which the puckering starts to move in front of the tip. This is supported by the fact that nanoscale strain relaxations are expected far quicker than the fastest scan rate used here (0.16 ms/nm) [23]. Therefore, escapes over the puckering ridge would lead to a significant relaxation of the surface, generating sharp slip events, at variance with the profiles reported here. This difference indicates that at $v > v_t$ the tip remains behind the puckered region, as originally predicted by finite element simulations [17].

Regardless the speed used, the probe-surface interaction potential ($V_P + V_S$) can be described by a metastable state of an escape potential barrier E_b and steepness β [Fig. 4(a)]. The speed dependence dynamics of friction is then determined by Kramer's rate: $\tau^{-1} = f_0 \exp[-E_b(t)/k_BT]$ [24], where f_0, for damped interacting systems [25], is close to lateral resonant frequency (kHz range) provided by the cantilever-tip-contact mechanics [6], and k_BT is the thermal energy. This rate is a measure of the average time needed to induce an escape over the barrier. At the beginning, just after the puckering formed, $E_b \gg k_BT$ and an escape over the barrier is unlikely. The tip can then displace along the stiff axis [black line in Fig. 3(d)]. Although such a displacement can depend on scanning speed, the barrier impeding the cantilever to return to its untwisted state remains nevertheless perpendicular to the scan axis.

At $v < v_t$, as the scanner advances slowly, a thermally activated escape becomes probable [left-hand side in Fig. 4(a)]. The distribution of the maximum friction force needed to induce a slip is hence expected to be narrow. This effect is enforced if β is low, because the barrier vanishes more quickly when the scanner moves further. With increasing v, the force behind the puckered region increases as there is less time for a thermally assisted escape. When the local stress approaches a critical pinning force the puckering can move in front of the tip eventually performing a partial relaxation. In this case the tip is not overcoming the top part of the barrier. Note that the unpinning process can also be subject to thermal fluctuations. This is similar to what occurs for lubrication films where stressed molecular blocks displace under the influence of an external sliding force [26].

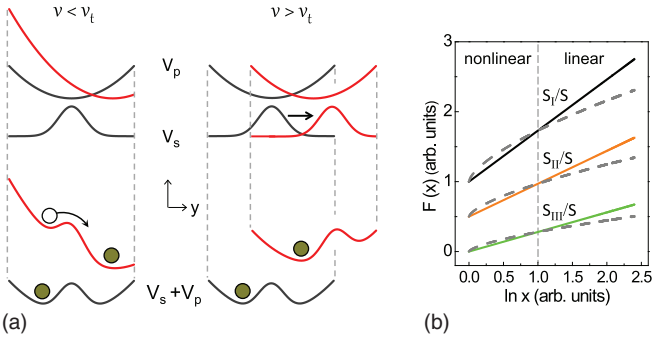

FIG. 4. (Color online) (a) Illustration of friction mechanisms below and above the threshold speed v_t. Upper part: Potential curves of the probe (quadratic lines) and of puckered surface (Gaussian-like lines) for two positions of the driving scanner (black vs red). Straight arrow indicates a forward displacement of the surface potential. Lower part: Positions of tip apex in the combined probe-surface interaction potential. The red curves are vertically shifted for shake of clarity. (b) Graphical representation of $G\times(-\ln x)^{2/3}$ and $G\times\ln x$ functions, where $G = S_I/S$, S_{II}/S, and S_{III}/S are the slopes of the linear parts in Fig. 3(b) and S is the slope for the domain of $|\theta| = 1°$. The pairs of curves are vertically displaced for clarity.

For any shape of the potential barrier the relationship between friction force F, temperature T, and v is given by [6,27]

$$\frac{1}{\beta k_B T}(F_c - F)^{1/p} = \ln\frac{v_c}{v} - \frac{1}{2}\ln\left(1 - \frac{F}{F_c}\right), \qquad (1)$$

where F_c is the friction force at zero temperature and v_c is a characteristic speed given by $v_c = (2f_0\beta k_BT)/(3k_{tot}\sqrt{F_c})$ at which thermal effects lose their impact, with k_{tot} the lateral stiffness of the cantilever-tip-contact ensemble. For $v \ll v_c$ and high temperature $F \ll F_c$, i.e., the last term in Eq. (1) is small. The $1/p$ power law accounts for the variation of E_b as a function of time via the dependence $E_b(t) = [(F_c - F)^{1/p}]/\beta$. In atomic scale friction [5], but also for other phenomena described by a transition rate [28], $1/p = 3/2$, because just before the barrier disappears, E_b varies more rapidly with distance. The friction force F thus scales with $[-\ln(v/v_c)]^{2/3}$. This also holds in our case for $v < v_t$. However, for $v > v_t$ the forward displacement of the barrier makes that the tip remains near the lower part of the potential well [right-hand side of Fig. 4(a)]. There $E_b(t)$ is better described by $(F_c - F)/\beta$ [5], i.e., $1/p = 1$. F depends then linearly on $\ln(v/v_c)$. For a comparison with our data, we show in Fig. 4(b) a graphical representation of the two analytical functions (dashed vs solid lines). Pairs of curves correspond to different prefactors, obtained by normalizing the slopes S_I, S_{II}, S_{III} measured for the three domains in Fig. 3(b) with S, the slope for the domain of $|\theta| = 1°$. In each case the two lines cross at a specific point defining two friction regimes, in good agreement with data from Fig. 3(b).

Additionally, according to Eq. (1), a high slope in Fig. 3(b) implies a large β value. So, when $|\theta|$ is heading to 60°, the potential barrier becomes steeper. This means, at fixed v, that the barrier takes more time to vanish. Hence, at the moment when the tip escapes over the barrier or the

puckering unpinning process takes place F is large, leading to a higher slope of the logarithmic variation. At variance with an atomic stick-slip case, where the interatomic distance fixes the periodicity of the potential barrier [29,30], here the width of the puckering can vary. Therefore, both an increase in height and/or a decrease in width of the initial potential barrier may lead to a steeper barrier profile. This can be in close relation with the tip path length on the ascending side of the ridge, which reduces when the ridge aligns more with the scan direction [blue line in Fig. 3(d)]. However, for domains with a ridge orientation close to the scan direction this effect starts to saturate due to the angular dependence. Then, a decreasing β can be understood by considering a lower barrier height. This can occur because of a weaker puckering induced by an additional axis—of same asymmetry as the stiff axis—which enters into play every 60°.

In conclusion, we reveal a significant speed-dependent spatial heterogeneity of nanoscale friction at the graphite surface. Our results put forward the puckering effect as an important friction and energy dissipation mechanism at this surface. This discloses ways for understanding and altering friction in sliding nanoscale contacts on lamellar materials. The effect used here to explain the dependencies of friction with speed can also be of interest to other dynamic critical phenomena, where potential barriers can spatially or energetically translate because of the thermal fluctuating driving force.

We acknowledge discussions with B. Heinrich and S. Le Roux. We also thank N. Beyer for technical assistance. This work is supported by Scientific Council of UdS (M.V.R.) and CPER (2007-2013) program.

[1] For a recent review on energy dissipation in friction see J. Y. Park and M. Salmeron, Chem. Rev. **114**, 677 (2014).
[2] I. Szlufarska, M. Chandronss, and R. W. Carpick, J. Phys. D: Appl. Phys. **41**, 123001 (2008).
[3] T. Bouhacina, J. P. Aimé, S. Gauthier, D. Michel, and V. Heroguez, Phys. Rev. B **56**, 7694 (1997).
[4] E. Gnecco, R. Bennewitz, T. Gyalog, Ch. Loppacher, M. Bammerlin, E. Meyer, and H.-J. Güntherodt, Phys. Rev. Lett. **84**, 1172 (2000).
[5] Y. Sang, M. Dubé, and M. Grant, Phys. Rev. Lett. **87**, 174301 (2001).
[6] E. Riedo, E. Gnecco, R. Bennewitz, E. Meyer, and H. Brune, Phys. Rev. Lett. **91**, 084502 (2003).
[7] A. E. Filippov, J. Klafter, and M. Urbakh, Phys. Rev. Lett. **92**, 135503 (2004).
[8] I. Barel, M. Urbakh, L. Jansen, and A. Schirmeisen, Phys. Rev. Lett. **104**, 066104 (2010); Phys. Rev. B **84**, 115417 (2011).
[9] A. Vanossi, N. Manini, M. Urbakh, S. Zapperi, and E. Tosatti, Rev. Mod. Phys. **85**, 529 (2013).
[10] M. V. Rastei, B. Heinrich, and J. L. Gallani, Phys. Rev. Lett. **111**, 084301 (2013).
[11] Z. Liu, J. Yang, F. Grey, J. Z. Liu, Y. Liu, Y. Wang, Y. Yang, Y. Cheng, and Q. Zheng, Phys. Rev. Lett. **108**, 205503 (2012).
[12] Z. Deng, A. Smolyanitsky, Q. Li, X-Q. Feng, and R. J. Cannara, Nat. Mater. **11**, 1032 (2012).
[13] R. Guerra, U. Tartaglino, A. Vanossi, and E. Tosatti, Nat. Mater. **9**, 634 (2010).
[14] T. Filleter and R. Bennewitz, Phys. Rev. B **81**, 155412 (2010).
[15] T. Filleter, J. L. McChesney, A. Bostwick, E. Rotenberg, K. V. Emtsev, T. Seyller, K. Horn, and R. Bennewitz, Phys. Rev. Lett. **102**, 086102 (2009).
[16] S. Kawai, T. Glatzel, S. Koch, B. Such, A. Baratoff, and E. Meyer, Phys. Rev. B **81**, 085420 (2010).
[17] C. Lee, Q. Li, W. Kalb, X.-Z. Liu, H. Berger, R. W. Carpick, and J. Hone, Science **328**, 76 (2010).
[18] J. S. Choi, J.-S. Kim, I.-S. Byun, D. H. Lee, M. J. Lee, B. H. Park, C. Lee, D. Yoon, H. Cheong, K. H. Lee, Y.-W. Son, J. Y. Park, and M. Salmeron, Science **333**, 607 (2011).
[19] J. S. Choi, J.-S. Kim, I.-S. Byun, D. H. Lee, I. R. Hwang, B. H. Park, T. Choi, J. Y. Park, and M. Salmeron, Rev. Sci. Instrum. **83**, 073905 (2012).
[20] P. Y. Huang, C. S. Ruiz-Vargas, A. M. van der Zande, W. S. Whitney, M. P. Levendorf, J. W. Kevek, S. Garg, J. S. Alden, C. J. Hustedt, Y. Zhu, J. Park, P. L. McEuen, and D. A. Muller, Nature (London) **469**, 389 (2011).
[21] Note that long linear deformations are unlikely at a precise moment, as puckering is limited to a finite area near the tip apex [17].
[22] Relevant here is the quadrant surface in front of stiff axis.
[23] A. Smolyanitsky, J. P. Killgore, and V. K. Tewary, Phys. Rev. B **85**, 035412 (2012).
[24] P. Hänggi, P. Talkner, and M. Borkovec, Rev. Mod. Phys. **62**, 251 (1990).
[25] A. Garg, Phys. Rev. B **51**, 15592 (1995).
[26] B. N. J. Persson, O. Albohr, F. Mancosu, V. Peveri, V. N. Samoilov, and I. M. Sivebaek, Wear **254**, 835 (2003).
[27] This expression has recently been slightly changed by considering a variable attempt frequency at speeds close to a critical point v_c at which friction saturates. The factor preceding the second logarithm was found 1/4 instead of 1/2: Y. Dong, D. Perez, H. Gao, and A. Martini, J. Phys.: Condens. Matter **24**, 265001 (2012). In our case the sliding speeds are well below v_c.
[28] See for example the case of flux quantization in superconducting rings: J. Kurkijärvi, Phys. Rev. B **6**, 832 (1972).
[29] C. M. Mate, G. M. McClelland, R. Erlandsson, and S. Chiang, Phys. Rev. Lett. **59**, 1942 (1987).
[30] S. Morita, S. Fujisawa, and Y. Sugawara, Surf. Sci. Rep. **23**, 1 (1996).